Materials Chemistry and Physics 259 (2021) 124008

Contents lists available at ScienceDirect

Materials Chemistry and Physics

journal homepage: www.elsevier.com/locate/matchemphys

Effect of Ni nanoparticles in Zn-Ni$_x$ advanced alloys synthesized by sintering reaction

José G. Miranda-Hernández [a,**], Héctor Herrera-Hernández [a], Heriberto Casarrubias-Vargas [a], Jesús Vargas-Hernández [a], Ricardo Miranda [b], Itzel P. Torres-Avila [c], Enrique Hernández Sánchez [c,*]

[a] Universidad Autónoma Del Estado de México, Centro Universitario UAEM Valle de México, Laboratorio de Investigación y Desarrollo de Materiales Industriales, Atizapán de Zaragoza, Estado de México, 54500, Mexico
[b] Gettysburg College, Pennsylvania, USA
[c] Instituto Politécnico Nacional, UPIBI, Departamento de Bioingeniería, Avenida Acueducto S/n Barrio La Laguna Ticomán, 07340, Ciudad de México, Mexico

HIGHLIGHTS

- The effect of Ni nanoparticles in the properties of Zn-Ni$_x$ advanced alloys was evaluated.
- The synthesis of Zn-Nix alloys is feasible for additions of Ni Nano and microparticles.
- Advanced alloys were synthesized in a short time by the mechanical milling process.

ARTICLE INFO

Keywords:
Nanoparticles
Zn-nix advanced alloys
Sintering
Microstructure
Mechanical properties

ABSTRACT

Zn–Ni$_5$, Zn–Ni$_{10}$, Zn–Ni$_{15}$, and Zn–Ni$_{20}$ advanced alloys were prepared by mechanical milling and synthesized by sintering reaction in solid-state. This research aims to study the effect of Ni nanoparticles on the microstructural and mechanical properties of the Zn-based alloys. The morphological evolution of the microstructure and phase's formation of Zn-based alloys were examined through the optical microscopy, X-ray diffraction, and SEM-EDS elemental mapping. Its mechanical properties such as hardness and Young's Modulus were determined by Vickers microindentation and the ultrasonic method, respectively. The results showed that the intermetallic phases were not formed during the mechanical milling process regardless of the working conditions (4 h, 200 rpm). These intermetallic phases only appeared after the sintering stage (357 °C, 1 h), which is associated to atomic diffusion and resulted in the formation of NiZn, Ni_3Zn_{22}, $NiZn_3$, Ni_5Zn_{21}, δ-NiZn, and γ-ZnNi phases. The microstructure, hardness, and Young's Modulus have significant changes, compared to the same materials synthesized with Ni microparticles. The results showed that the mechanical properties were affected due to the addition of Ni.

1. Introduction

The Zn is a metallic material that has been used in several applications due to its properties such as low density, low electrical conductivity, and low melting point. Therefore, the Zn has been used in some essential industries like the automotive, shipbuilding, light elements, batteries, among others. Although the Zn is a very interesting material and it has valuable mechanical properties, its use is limited due to low hardness. However, the mechanical properties can be improved if the Zn is combining with other metals to form alloys. The improvement of the mechanical and chemical properties in the Zn based alloys allows have to new industrial applications and increases its commercial value as is mentioned by F. M. Azizan et al. [1]. Originally Zn was alloyed with cadmium; nevertheless, due to the harsh environmental conditions associated with cadmium, it has been necessary to analyze other metals instead of cadmium according to H.Y. Lee and S. G. Kim [2] and P.

* Corresponding author.
** Corresponding author.
E-mail addresses: jgmirandah@uaemex.mx (J.G. Miranda-Hernández), enriquehs266@yahoo.com.mx (E.H. Sánchez).

https://doi.org/10.1016/j.matchemphys.2020.124008
Received 2 September 2019; Received in revised form 20 August 2020; Accepted 3 November 2020
Available online 6 November 2020
0254-0584/

Ganesan et al. [3]. The Zn base alloys can be formed in several ways, such as Zn–Ni, Zn–Fe, Zn–Co, Zn–Ni–Co, and Zn–Ni–Fe. In particular, Zn– Ni alloys were mainly developed as a replacement for cadmium because Ni is cheap and easy to work according to Heidi A. Conrad et al. [4]. Ni presents excellent corrosion resistance due to the formation of several complex products during the manufacturing process (phases of the Zn-Nix system) which act as a barrier against corrosion propagation as is mentioned by G. Barceló et al. [5], M. E. P.Souza et al. [6], and R. Rizwan et al. [7]. When Zn and Ni are alloyed, several intermetallic phases are formed regardless of the synthesis method due to the weight percent of Ni in the system, such as η-(1% wt. Ni), α and β-(30% wt. Ni, known as the Ni-rich phases), δ-(Ni_3Zn_{22}) and ɣ-(Ni_5Zn_{21}) known as the Zn-rich phases according to Ref. [4,7], J.B. Bajat et al. [8], A. Petrauskas et al. [9], and H. Okamoto et al. [10]. Each stage affects the alloy; for example, the intermetallic ɣ phase alloy offers the best corrosion resistance, with the Ni content between 8 and 15% wt [4,8]. Likewise, the mechanical property as hardness, show changes with the addition of amounts of Ni in the Zn–Ni system [7]. Others studies reported the use of these alloys as biodegradable materials as is mentioned by E. Mostaed et al. [11], as well as the possibility of fabricating metallic alloys and intermetallic compounds of Zn–Ni by using procedures like immersion in chloride salt-baths [5], sintering method reported by C. Gang et al. [12] and N. Setoudeh et al. [13], and mechanical alloying discussed by S. Bid and S.K. Pradhan [14], J. Park et al. [15], J. M. Kim and J. S. Park [16], Kahtan S. Mohammed and Haider T. Naeem [17], and M.A. Ahmed et al. [18], these studies are based on the analysis of microstructural changes such as catalysis, mechanical behavior, thermodynamics, and electrical properties of the alloys as is reported by G. Penev Vassilev et al. [19] and T. Lee et al. [20]. On the other hand, there are many investigations on Zn–Ni alloys synthesized by the electrochemical method, where the microstructural behavior, hardness, thermal stability, corrosion resistance, and hydrogen permeability of Zn–Ni electrodeposit that has been also studied and discussed by R. Fratesi et al. [21], J. Giridhar et al. [22], W. A. Badawy et al. [23], Y. Boonyongmaneerat et al. [24] and F. J. Fabri Miranda et al. [25]. Another method widely used for the synthesis of Zn–Ni alloys is the mechanical alloying process, this process is also used as an alternative for the processing of materials such as alloys, composites, intermetallic materials, and ceramics (even when requires a high amount of time) according to V. Viswanathan et al. [26], R. A. Rodríguez-Díaz et al. [27], K. Hyun-Su et al. [28], and C. Carreño-Gallardo et al. [29]. Furthermore, several researchers cited in Refs. [14,16,17,26–29] and Edval G. Araujo et al. [30] showed that it is possible to obtain materials with good density, uniform microporosity, high hardness, and fracture toughness values, high Young's modulus, and other properties using mechanical alloying and sintering process.

Therefore, this work focuses on the investigation of the effects of Ni nanoparticles added in the binary Zn base alloy, through a non-equilibrium method such as mechanical milling and material consolidation by a sintering process. The research aims to produce materials, which cannot be obtained by conventional manufacture procedures due to its melting temperature differences between the alloy components. This research considers two fundamental interests; first, the synthesis of Zn–Ni alloys, the microstructural analysis, and evaluation of the mechanical properties (microhardness and elastic modulus). Second, and as future work is to evaluate the viability to use this material as energy cells because of the hydrogen evolution reaction, considering the literature information related to the use of Ni-base alloys is feasible, as is reported by Ref. [17,23], H. Herraiz-Cardona et al. [31], M.J. De Giz et al. [32], and J. Divised and H. Schmitz [33].

2. Experimental procedure

2.1. Samples preparation

Powders reagent grade of Zn (99% purity, mesh #200, J.T. Baker) and Ni nanoparticles (99% purity, ≤100 nm, Aldrich) were used to form the chemical compositions according to Zn-Ni_x (x = 5, 10, 15, and 20 wt %), where x is the percent by weight of Ni addition in the Zn base alloys. The powder mixtures were subjected to a mechanical milling process using a high-energy planetary ball-mill ("FRITSCH," Pulverisette 6) at 200 rpm during 4 h. In this process, an agate cylindrical-container and agate balls of 10 mm in diameter were used, the relation of powder-balls was 10:1 in wet condition using isopropyl alcohol (C_3H_7OH) as the controlling process agent. Subsequently, the powder mixtures were uniaxially compacted in a cylindrical shape of 20 mm of diameter and 2 mm thickness by applying a total pressure of 300 MPa at room temeparature. The compacted samples were consolidated by a solid-state sintering treatment at a heating rate of 10 °C/min in an electric furnace (Nabertherm, LHT 02/18). The established sintering temperature was 357 °C during 1 h in the presence of a nitrogen-controlled atmosphere.

2.2. Microstructural characterization

The bulk density and apparent porosity of the sintered powders were determined according to Archimedes' method at room temperature. The surface of the sintered compacts was prepared using standard metallographic procedures. The corresponding microstructure was examined by optical microscopy (OM) with an OLYMPUS, GX51 and by scanning electron microscopy (SEM) with a JEOL, JSM6300 equipped with an energy-dispersive X-ray spectrometer (EDS) detector. The EDS assay was used to analyze the elemental contents (mapping) operating with an acceleration voltage of 15 kV applied to a working distance (WD) of 7.2 mm. X-ray diffraction (XRD) analysis of the samples was performed in a diffractometer (BRUCKER, D8 ADVANCED), using Kα of Cu monochromatic radiation (λ = 1.5406 Å) at a scan rate of 4°/min to identify the crystalline phases in the powder mixture alloy.

2.3. Mechanical characterization

The hardness of the sintered samples was determined by using the Vickers microindentation technique (EMCOTEST, DURASCAN-20). Finally, the elastic modulus (E_{us}) was determined through the ultrasonic method according to Eq. (1).

$$E_{us} = v_{us}^2 \rho_m \quad (1)$$

Where E_{us} is the ultra-sonic elastic modulus (GPa), v_{us} is the supersonic speed (ms^{-1}) in a longitudinal direction and ρ_m is the density of the material ($kg\ m^{-3}$).

3. Results and discussion

3.1. Microstructural analysis

According to the experimental procedure, the powders from all chemical systems were compacted in cylindrical samples and then subjected to a sintering process under the conditions previously mentioned. Fig. 1 shows the different alloys obtained after the sintering process corresponding to the Zn–Ni_5, Zn–Ni_{10}, Zn–Ni_{15}, and Zn–Ni_{20} system from left to right, respectively. Changes in color after the sintering process are related to increases of Ni in the Zn–Ni system.

On the other hand, based on the Zn-Nix system as the motive of this work, the possible formation of the intermetallic phases was assumed. According to the binary phases-diagram Zn–Ni (see Fig. 2) that was consulted and showed by H. Okamoto et al. [10], J. C. Sabol et al. [34] and W. Xiong et al. [35], the intermetallic phases such as ɣ and δ can be formed in the synthesized materials using 5, 10, 15 and 20% in wt. of Ni addition in the Zn base material. In particular, J. C. Sabol et al. [34] says that the intermediate ɣ and δ phases can be formed in the range of ~73–~86 wt% Zn and ~89.5 to ~91.0 wt% Zn respectively.

After the mechanical milling process, the powders of all chemical

Fig. 1. Samples of Zn–Ni_5, Zn–Ni_{10}, Zn–Ni_{15}, and Zn–Ni_{20} after sintering process, respectively.

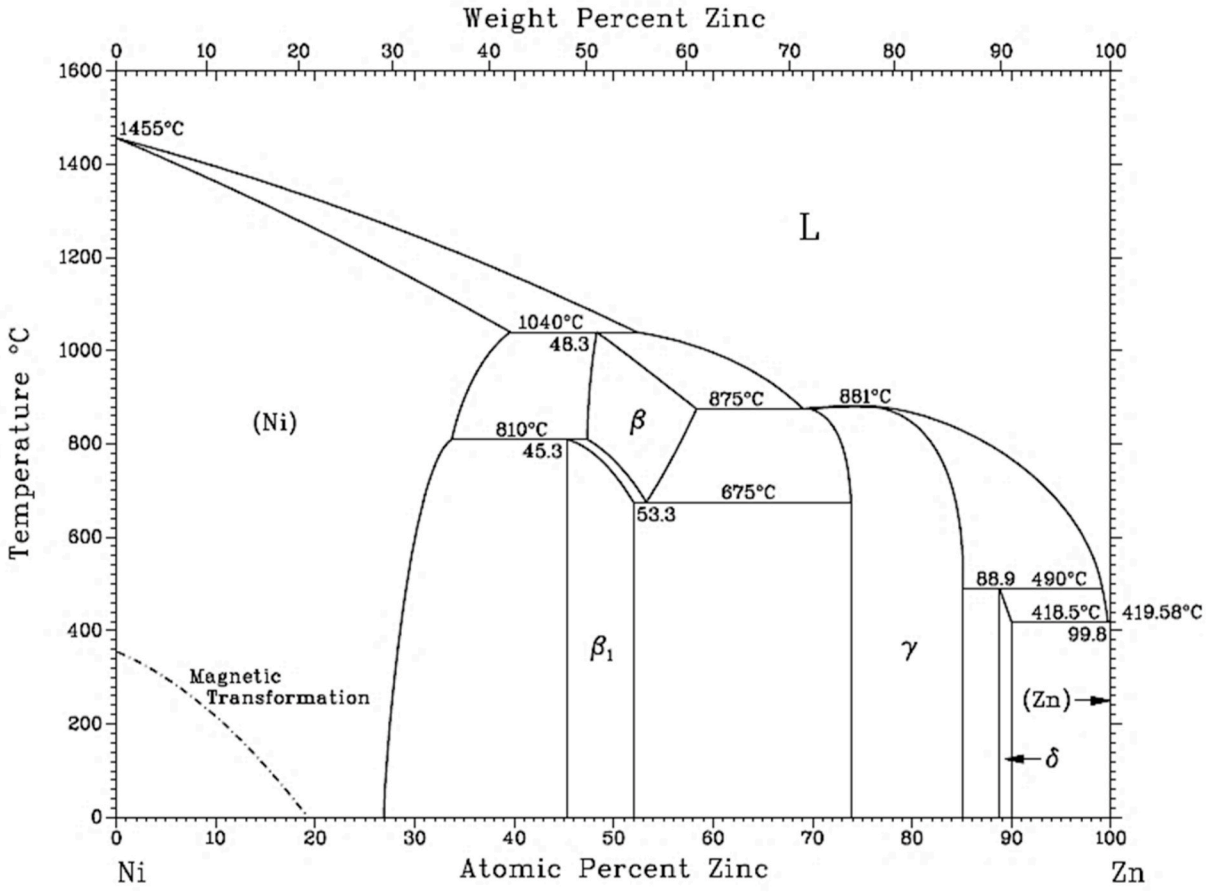

Fig. 2. Phase diagram Zn-Ni [34].

compositions were analyzed by XRD, the results identified the characteristic peaks of the precursor materials Zn, Ni, and a trace of ZnO, but Zn–Ni alloy phases was not identified in the XRD patterns. The cause of the non-formation of the Zn–Ni alloy phases during the mechanical milling process could be the working conditions (4 h., 200 rpm), which were lower than those reported by other researchers. That is, the intermetallic phase ɣ-ZnNi was formed by the mechanical milling process until 200 working hours according to J. Park et al. [15], the synthesis of other similar alloys using 15 h of mechanical milling process was also reported by H. Tawfiq Naeem [36].The formation of ZnO is due to the presence of air in the container during the milling process, despite that for the control of the chemical composition in this process, a vacuum box was used.

In this sense, Fig. 3 shows the XRD patterns of the sintered samples according to Zn-Ni_x system alloys. The results were indexed with JCPDS cards, and the formation of intermetallic phases was identified in all systems. Fig. 3a shows the formation of intermetallic phases such as NiZn, Ni_3Zn_{22}, δ-NiZn, $NiZn_3$, and Ni_5Zn_{21} corresponding to Zn–Ni_5 alloy after the sintering process. Fig. 3 (b), (c), and (d) corresponding to the Zn–Ni_{10}, Zn–Ni_{15}, and Zn–Ni_{20} alloys respectively, show the formation of the intermetallic phases (NiZn, Ni_3Zn_{22}, δ-NiZn, $NiZn_3$, and Ni_5Zn_{21}) including a new intermetallic phase as ɣ-Zn_2Ni_{11} that was not identified in the Zn–Ni_5 alloy. Nevertheless, the formation of several intermediate Zn–Ni phases can be explained because during the mixed in the mechanical milling process the Zn and Ni cannot be distributed homogeneously, i.e., there are Ni-rich zones that during the sintering process allow the formation of possible intermediate Zn–Ni phases due to the equilibrium conditions in the Zn-Ni_x formed systems. The ZnO phase was also identified after the sintering process in all Zn-Nix system alloys. It is clear that although in the experimental process, the oxidation of the powder samples was controlled through of inert gas atmosphere, oxygen can be diffused from the environment towards the metal powder samples during its handling.

Considering our previous work in the synthesis of Zn-Nx with the same conditions but using Ni microparticles, the Zn, Ni_3Zn_{22}, and ɣ-Zn_2Ni_{11} phases in all chemical systems were also identified, these results were reported elsewhere by José G. Miranda-Hernández et al. [37]. According to the results, the difference is that in the alloys synthesized

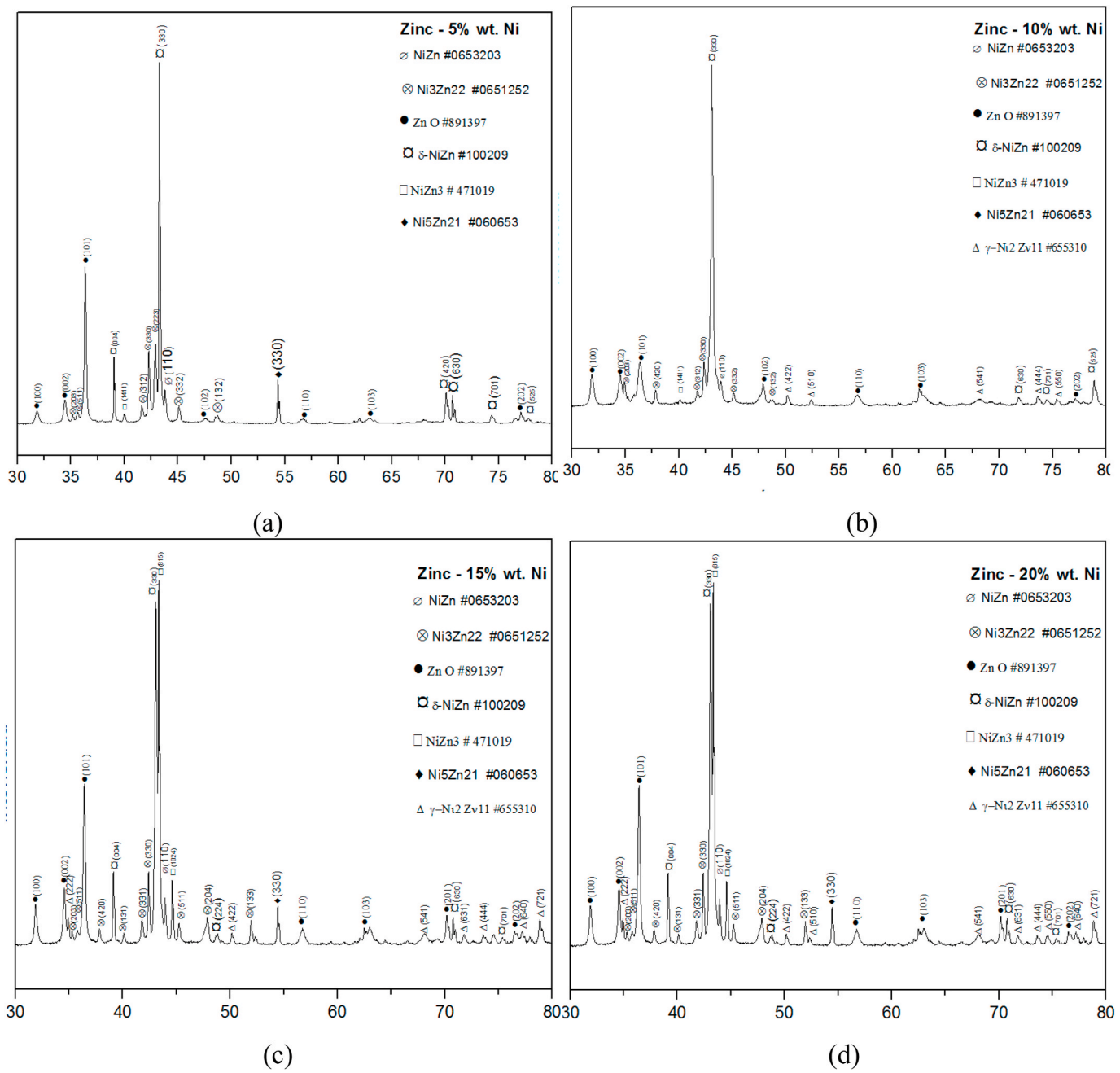

Fig. 3. XRD patterns of the Zn-Ni_X system sintered with Ni nanoparticles: (a) Zn–Ni_5, (b) Zn–Ni_{10}, (c) Zn–Ni_{15}, and (d) Zn–Ni_{20}.

with Ni nanoparticles there is the presence of the δ-NiZn, $NiZn_3$, and Ni_5Zn_{21} intermetallic phases that were not formed in the Zn–Ni alloys synthesized with Ni microparticles. Although the Zn phase no appears in the alloys synthesized with Ni nanoparticles. This behavior can also be associated with the oxidation phenomenon due to the introduction of oxygen in the crystalline lattice of Zn/ZnO, in consequence, the oxygen causes a strong structural distortion and lattice deformation resulting in the formation of an amorphous structure, i.e., the Zn present in the original chemical systems oxidizes during the process but also forms the intermetallic phases.

Alternatively, the alloys were analyzed by SEM-EDS. In particular Fig. 4 shows the micrographs SEM-EDS which corresponds to the Zn–Ni_5 alloy and three interesting zones can be appreciated, this alloy is taken as an example to show the behavior in all alloys. The EDS patterns identified Zn and Ni at each point. Also, EDS elemental maps by X-ray fluorescence identified the distribution of the Ni phase in the Zn-base material, where Ni was identified as blue dots segregated and homogeneously dispersed throughout the entire Zn matrix. Similar behavior was observed in all chemical compositions (Zn–Ni_{10}, Zn–Ni_{15}, and Zn–Ni_{20}) synthesized with nanoparticles. The physical phenomenon that allows the consolidation of these materials and the formation of the Zn–Ni phase is the atomic diffusion mechanism of Zn in the Ni matrix through the grain boundary. However, it should be considered that Ni has a higher melting point than Zn, but the Zn represents the main proportion of %wt. in the systems, and the relationship between the sintering temperature and melting point is about 85%, which are favorable conditions to promote a faster diffusion of Zn at high energy to achieve higher densification of the materials.

On the other hand, taking information about our previous investigation only for comparison, Fig. 5 shows the SEM-EDS analysis of the material sintered with Ni microparticles that was reported by José G. Miranda-Hernández et al. [37]. In Fig. 5, area 1 corresponds to the

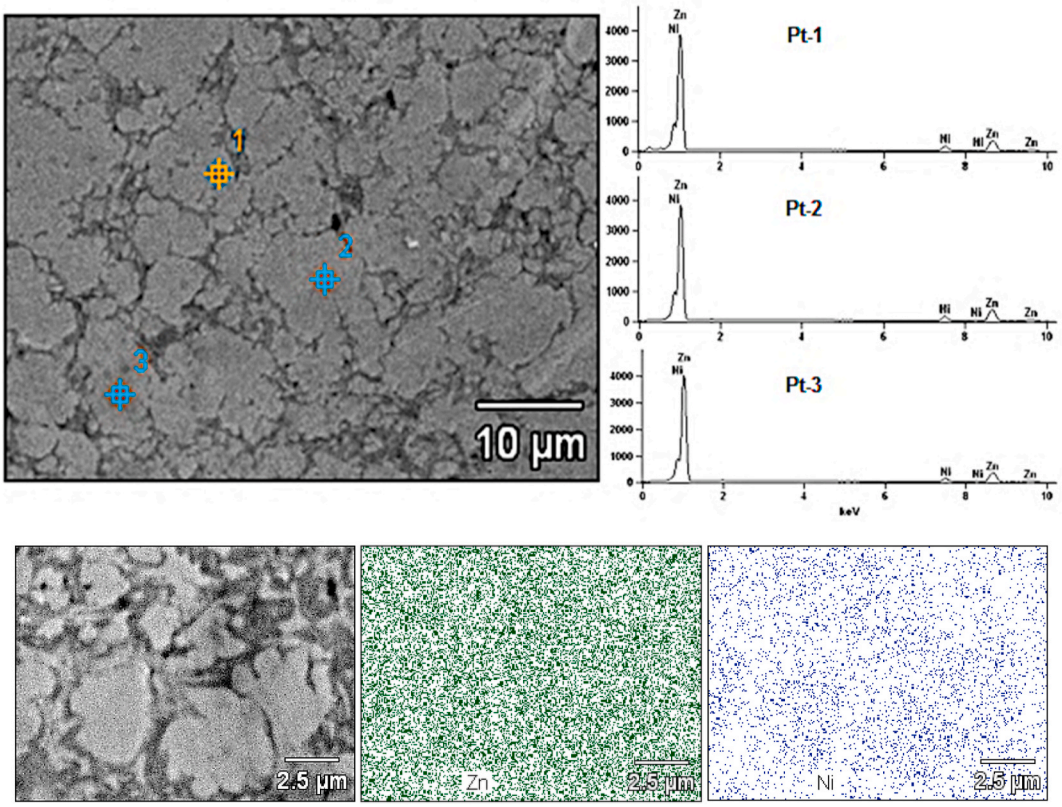

Fig. 4. SEM micrograph, EDS spectra and EDS elemental maps by X-ray fluorescence of Zn–Ni_5 alloy sintered with nanoparticles, show the identified and the distribution Zn and Ni elements.

central isolated as a dark-gray phase, which is identified with higher intensity of characteristic Ni peaks, while area 2 consists of alternated peaks of Zn and Ni as a light-gray phase (Zn–Ni). The metal matrix of Zn was identified in areas 3 and 4. Through EDS elemental maps by X-ray fluorescence, the Ni phase (dark-gray) corresponds to the isolated phase surrounded by the Zn–Ni phase (light-gray) was identified, according to this Figure Ni was also identified as blue dots segregated and finely dispersed throughout the entire Zn matrix (dark-green dots). Finally, in the comparison, the main difference between Zn-Nix alloys synthesized with Ni nanoparticles and Ni microparticles reported by José G. Miranda-Hernández et al. [37] is that the alloys prepared with Ni nanoparticles do not form phases of isolated areas, the Ni and Zn are homogeneously distributed in the matrix to forms Zn–Ni intermetallic phases in all material, and the alloys synthesized with microparticles present areas of Zn–Ni intermetallic phase between a Zn phase and other Ni phase.

Instead, Fig. 6 shows the microstructure of a reference sample of pure Zn synthesized under the same work conditions and Fig. 7 shows the microstructure of the alloys obtained by optical microscopy. In these micrographs is possible to observe the porosity and the superficial morphology. It is possible to observe that the porosity is distributed along the Zn-matrix, which increases with the addition of Ni nanoparticles. On the other hand, the microstructures of Zn-Nix system, present one light-gray phase formed by precipitates of the Ni material, and a second dark-gray phase that corresponds to the Zn-base content, as can be observed in Fig. 7(a), (b), (c) and (d). The assumption that the light-gray phase could be caused by the addition of Ni particles is because it does not appear in the microstructure of pure Zn (see Fig. 6).

In this sense, Fig. 8 shows the microstructures obtained by José G. Miranda-Hernández et al. [37] of the alloys base Zn with Ni microparticles. These microstructures are utterly different from those sintered with Ni nanoparticles, as well is mainly observed coarser particles that precipitate as a light-gray phase with a semi-spherical shape. Those semi-spherical shape particles possibly correspond to the Ni phase because they are more noticeable when the content of this component increases. Also, a second phase is observed as a dark-gray phase, which corresponds to Zn-base material. Moreover, the increase of the porosity and the microstructural modification during the synthesis of Zn-Nix alloys is based on the assumption that the phase's formation occurs during the material's consolidation due to; the diffusion phenomena in a solid-state, the temperature effect, and the content of Ni (wt.%) present in the system.

On the other hand, the microstructure of the Zn–Ni_5 alloy synthesized with Ni nanoparticles (Fig. 7a) have a closed microporosity in comparison whit the porosity of the Zn–Ni_5 system alloy synthesized with Ni microparticles (Fig. 8a); this fact is attributed to the fast diffusion of Zn at the temperature of 357 °C, due to it is very close to the melting temperature of the Zn (419.53 °C). While that in the Zn–Ni_{10}, Zn–Ni_{15}, and Zn–Ni_{20} (Fig. 7) alloys synthesized with nanoparticles and the Zn–Ni_{15} alloy synthesized with microparticles (Fig. 8b), the size of the pores was more evident when the Ni content in the alloy increases. This behavior is due to the higher difference between the melting temperature of Ni (1455 °C) than the sintering temperature making the Ni diffuses slowly and leaving more structural defects, although it is notable that the porosity in both systems is different. Generally, the microstructural differences of the compounds after sintering are remarkable compared to the microstructure of pure Zn. Therefore, it can be observed that the microstructural morphology of the materials is a function of the quantity and particle size of Ni present in the system and it is also a peculiar characteristic of the materials manufactured by powder metallurgy.

Finally, when the Ni particles were added in the Zn-Nix over to 15% wt., it is possible to observe the intermetallic phases formed in the alloys, as shown in Fig. 9. A similar microstructure is observed in the alloys sintered with Ni microparticles [37] and Ni nanoparticles, but the latter with a finer microstructure (Fig. 9a). In this sense, a close

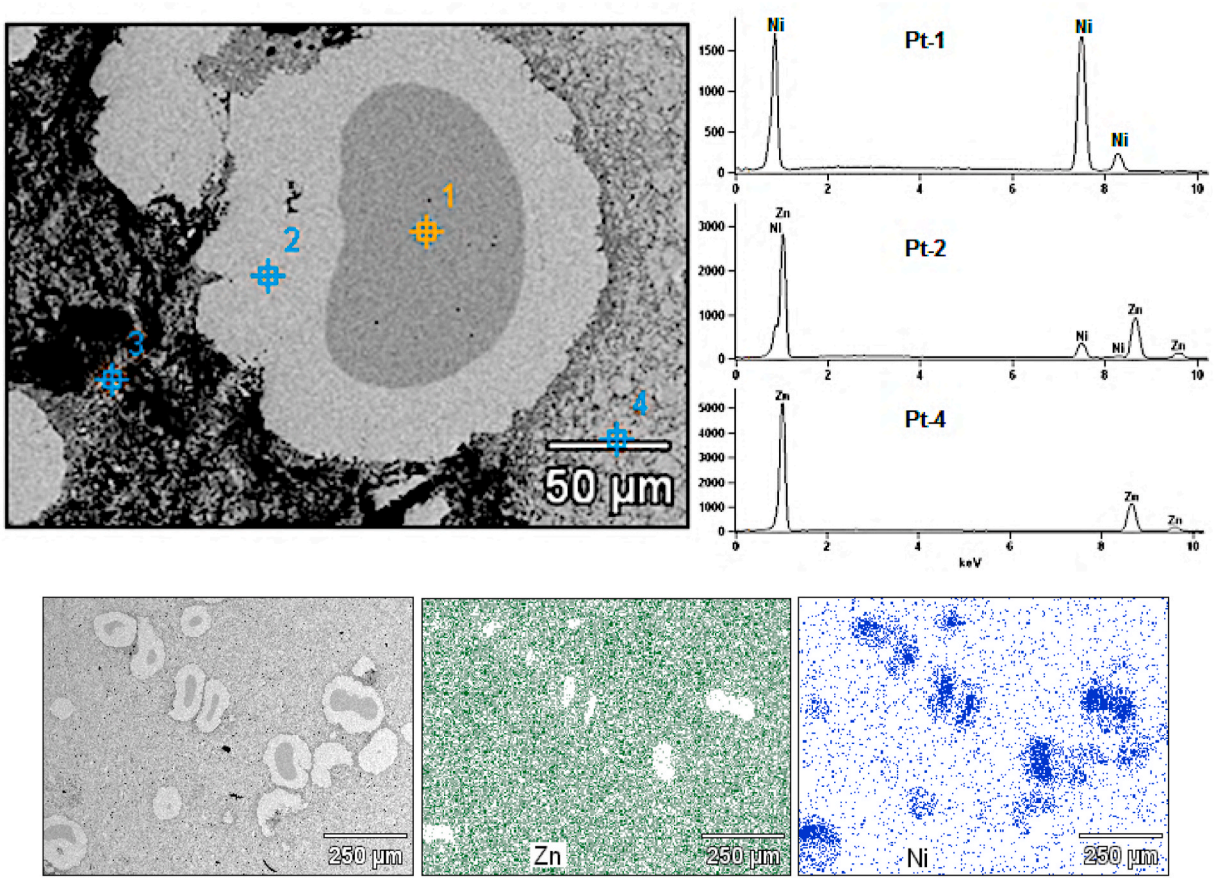

Fig. 5. SEM micrograph, EDS spectra and EDS elemental maps by X-ray fluorescence of Zn–Ni_5 sintered with nickel microparticles, show the identified and the distribution Zn and Ni elements.

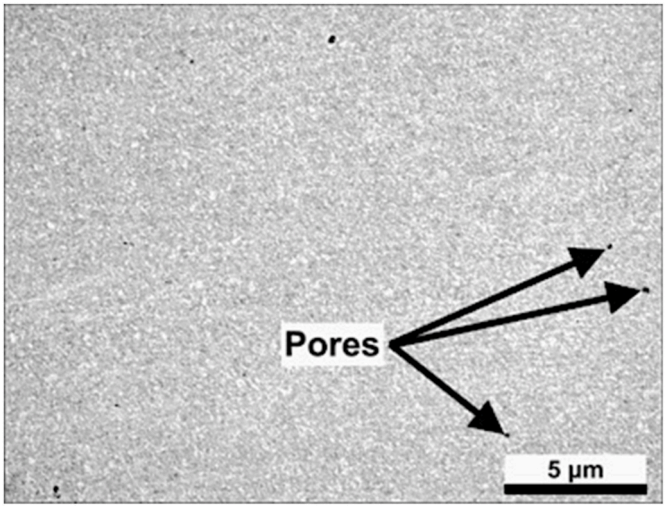

Fig. 6. Optical image of the microstructure of pure Zn.

inspection by optical microscopy shows the microstructural details in the Zn–Ni_{15} alloys (Fig. 9). In these microstructures, it is clear that the Ni phase is surrounded by the supposed Zn–Ni intermetallic phase in both systems, In similar works with alloys base Zn, the researchers J.A. Aragón et al. [38] and J.A. Aragón and J.R Miranda [39] reported the formation of precipitates embedded within of the matrix material. Also possible to observe the presence of micropores and the Zn phase which corresponds to the base material. According to this observation, it is assumed that the intermetallic Zn–Ni phases grow during the sintering process on pre-existing sites, in which the interfacial energy is the lowest for nucleation and growth mechanism, instead of forming during mechanical milling of the powder.

3.2. Density and porosity

The density and porosity of the resulting compounds were determined by the Archimedes method in a vacuum environment on all alloys (see Table 1). In general, the density has an increase in all compositions with a relation directly proportional to the increase of Ni. This behavior is associated with the addition of more dense material (Ni = 8.90 g/cm^3) than Zn (7.14 g/cm^3) in the structure of Zn-Nix, but also to the consolidation of the materials due to the sintering process. The density in the different alloys is similar, although the density values of the alloys fabricated with Ni nanoparticles are slightly above that of the composites manufactured with Ni microparticles, according to the values reported by José G. Miranda-Hernández et al. [37].

On the other hand, the experimental density moves away from the theoretical density having as a consequence, a diminish in the percent of densification (see Fig. 10). The results around density and porosity can be possibly explained by the diffusion of Zn or Ni particles in the alloy matrix, which contributes to the consolidation of the materials due to the Zn–Zn, Zn–Ni, and Ni–Ni particles interactions. Those interactions should be caused because of the large ratio of melting points between the Zn-matrix and the reinforcement Ni-phases particles. However, at the temperature about 357 °C in which the process of sintering occurs, Ni atoms diffuse very slowly in the Zn structure, this behavior could be attributed to the significant differences in melting temperatures of both compounds according to José G. Miranda-Hernández et al. [37] and J. A.

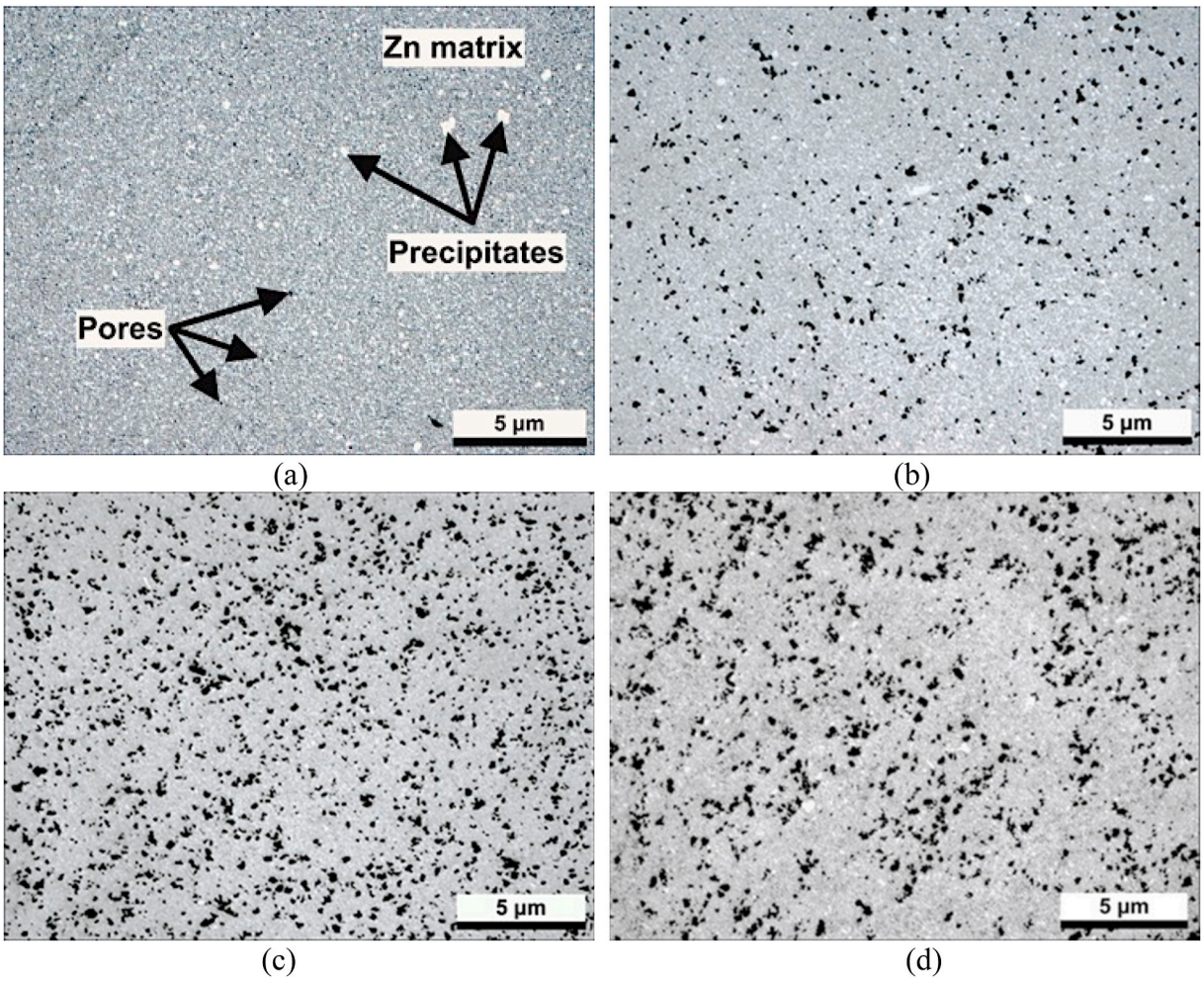

Fig. 7. Optical microstructures obtained at magnification 5× in the system Zn-Ni_X sintered with Ni nanoparticles: (a) Zn–Ni_5, (b) Zn–Ni_{10}, (c) Zn–Ni_{15}, (d) Zn–Ni_{20}.

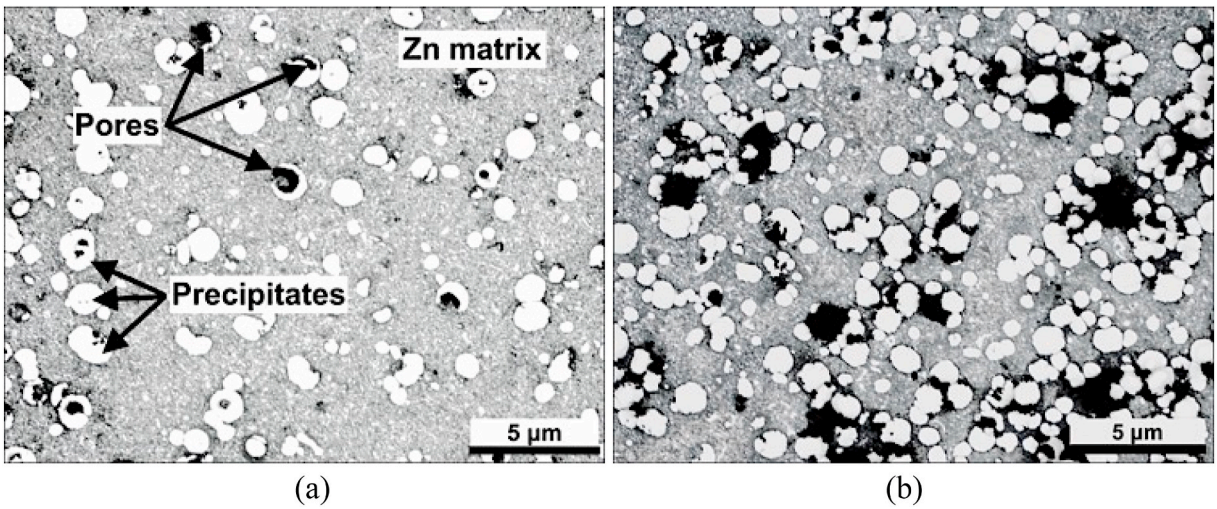

Fig. 8. Optical microstructures obtained at magnification 5× in the system Zn-Ni_X sintered with Ni microparticles respectively: (a) Zn–Ni_5, (b) Zn–Ni_{15}.

Aragón et al. [38]. As well, Fig. 10 shows the ratio between densification and porosity of the materials after being sintered. For example, the Zn–Ni_5 alloys have a densification value of 90.4%, which is higher than the Zn–Ni_{20} value (88.7%) in the system synthesized with Ni nanoparticle. Similar behavior can be observed in the materials fabricated with Ni microparticles [37]. Hence, when the Ni addition increases, the percent of the densification decreases, and this behavior seems to be inversely proportional to the percent of the porosity.

3.3. Hardness and young modulus

The hardness values of all synthesized materials were determined

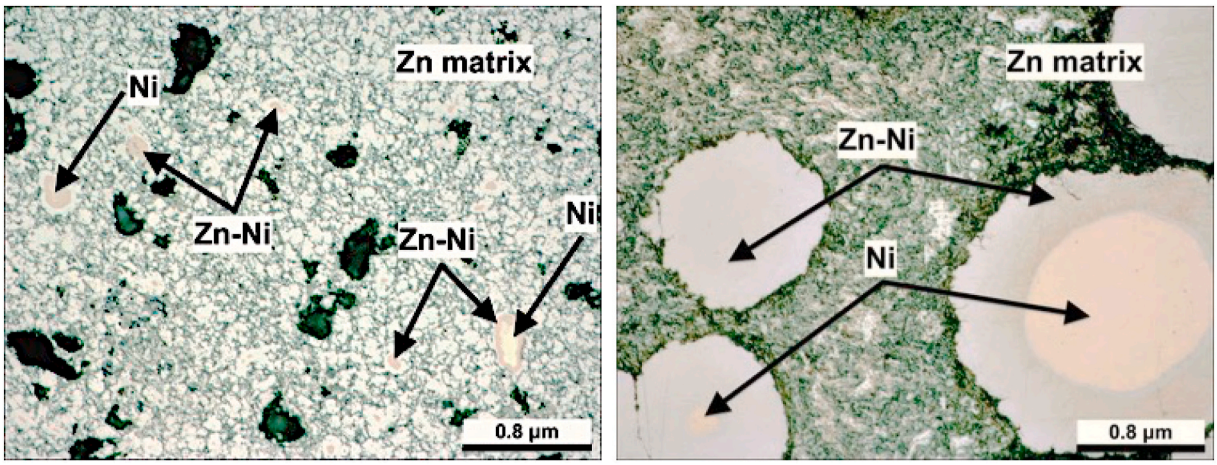

Fig. 9. Microstructures (50× magnification) of Zn–Ni_{15} sintered with nanoparticles and microparticles respectively showing the Zn–Ni intermetallic phase.

Table 1
Density of Zn-Ni_X system alloys.

System Zn-Ni_X	Zn	Zn–Ni_5	Zn–Ni_{10}	Zn–Ni_{15}	Zn–Ni_{20}
Theoretical Density (mix rule)					
ρ_t /(g/cm^3)	7.13	7.22	7.31	7.40	7.48
Density values of alloys synthesized with nanoparticles					
ρ_n /(g/cm^3)	6.52	6.54	6.57	6.59	6.64

considering the average of 30 measures in each sample. The hardness determined in the sample with pure Zn was 62 ± 5 H V and this value can be taken as a reference for observing the effect of the Ni addition in the Zn-base material. Therefore, in this research was found that the hardness does not increase in the Zn–Ni_5, Zn–Ni_{10}, Zn–Ni_{15}, and Zn–Ni_{20} systems when the Ni increases, *i.e.,* the hardness is not a function of the Ni addition in the alloys, as shown in Table 2. But consider that the hardness values of the alloys fabricated with Ni nanoparticles were higher than those obtained for the alloys synthesized with Ni microparticles according to José G. Miranda-Hernández et al. [37]. The hardness of the Zn-Nix alloys with Ni nanoparticles is 4 times mayor on average than the Zn pure. On the other hand, R. Rizwan et al. [7] reported that the hardness decreases with the presence of Ni in the Zn–Ni alloys, also researchers as J. A. Aragón et al. [38] observed changes in the hardness of Zn base alloys due to the addition of Cu in the system.

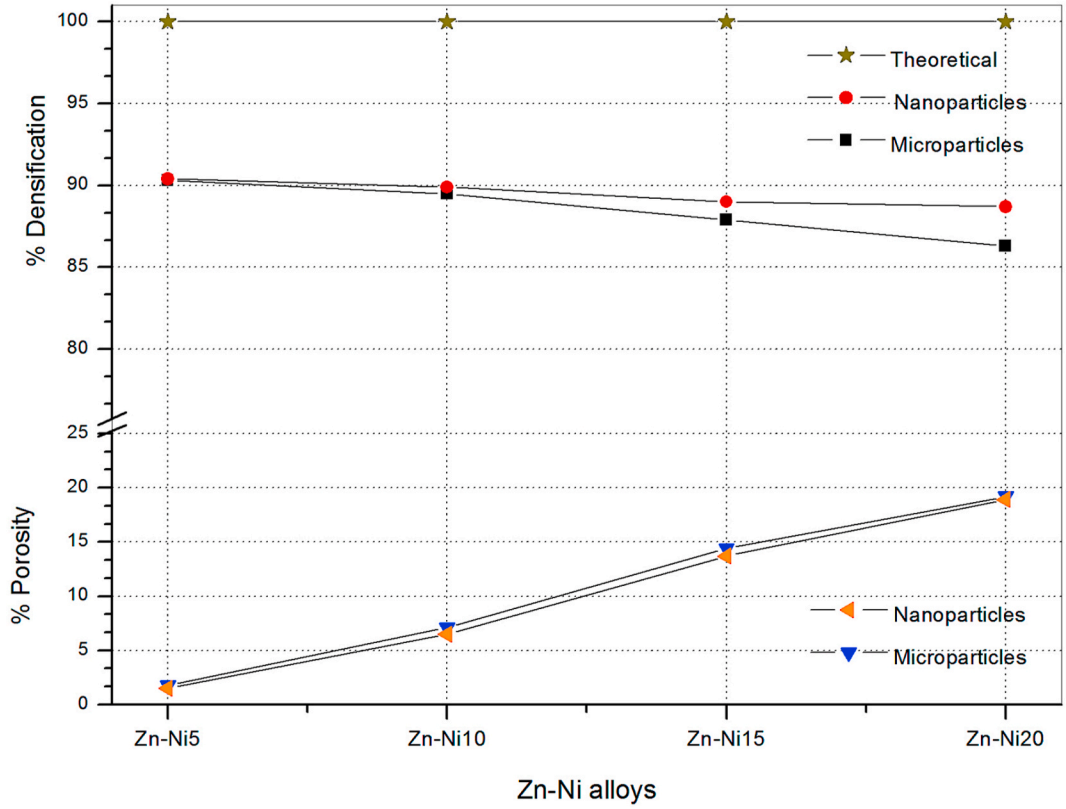

Fig. 10. Densification behavior and porosity from powder alloys of Zn-Ni_X.

Table 2
Hardness values of the materials synthesized.

Zn-Ni$_X$ system	Zn–Ni$_5$	Zn–Ni$_{10}$	Zn–Ni$_{15}$	Zn–Ni$_{20}$
Hardness (HV)	239 ± 9	244 ± 5	240 ± 7	238 ± 10

Fig. 11 shows the microstructures of Zn–Ni$_{15}$ alloys synthesized with Ni nanoparticles and Ni microparticles as a reference to the hardness behavior in all materials. The micrographs show the different zones where hardness was measured, *i.e.,* are notables the indentation prints on the intermetallic Zn–Ni phase, Ni-rich phase, and Zn-rich area (metallic-matrix) according to the images. However, the hardness values varied according to the region where it was measured. For example, in the materials synthesized with Ni nanoparticles and Ni microparticles, the average hardness values in the zone considered as the Zn phase were 117 ± 14 H V and 63 ± 4 H V [37], respectively. Namely, the hardness value in the Zn phase of synthesized materials with Ni nanoparticles are larger than synthesized alloys with Ni microparticles. This behavior is due to the formation of Zn–Ni microphases less than 25 μm where these microphases are smaller than the size of the phase formed in the synthesized alloys with Ni microparticles (approximately 100 μm), as shown in Fig. 11 (b) and (d). Another explanation is due to the possible formation of Zn–Ni nanophases during the sintering process and also the homogeneous distribution of Ni nanoparticles in the chemical composition during the mechanical milling process, considering that the average hardness of the Zn–Ni phase was 382 ± 27 H V in the materials synthesized with Ni nanoparticles and 416 ± 10 for materials synthesized with Ni microparticles [37]. Likewise, a clear difference in the indentation size can be observed in Fig. 11 (a) compared to those observed in Fig. 11 (c), considering that the load applied (0.49 N) was the same. The difference in the indentation size is due to the change of the hardness in the materials, but also can be attributed to a variety of phenomena, including work hardening during indentation, loading to initiate plastic deformation, the elastic indentation recovery, plastic deformation band spacing, and the effect of the distorted zone according to G. Rodríguez-Castro et al. [40].

Finally, Young's modulus or elastic modulus (E_{us}) of the obtained phases was estimated considering the theoretical values of E for Zn as 104.5 GPa and 82 ± 4 GPa for the reference sample. The obtained values of E_{us} are summarized in Table 3. It can be observed that the behavior of the elastic modulus is directly related to the increasing of Ni content in the Zn-Nix systems. Note that the E_{us} values in these alloys are under the theoretical value and the reference sample. The incorporation of Ni in the matrix Zn has an apparent effect in E_{us}; the alloys synthesized have an exciting behavior because the E_{us} tends to increase when the %Ni increase. This change can be considered as a good advantage due to a decrease in the elastic modulus results in materials more apt to face elastic deformation.

Finally, the incorporation of Ni in Zn-Nix system, in general, has a

Table 3
Young's modulus values of the materials synthesized with Ni nanoparticles.

Zn-Ni$_X$ system	Zn–Ni$_5$	Zn–Ni$_{10}$	Zn–Ni$_{15}$	Zn–Ni$_{20}$
Young's modulus (E/GPa)	17 ± 2	18 ± 1	27 ± 1	36 ± 3

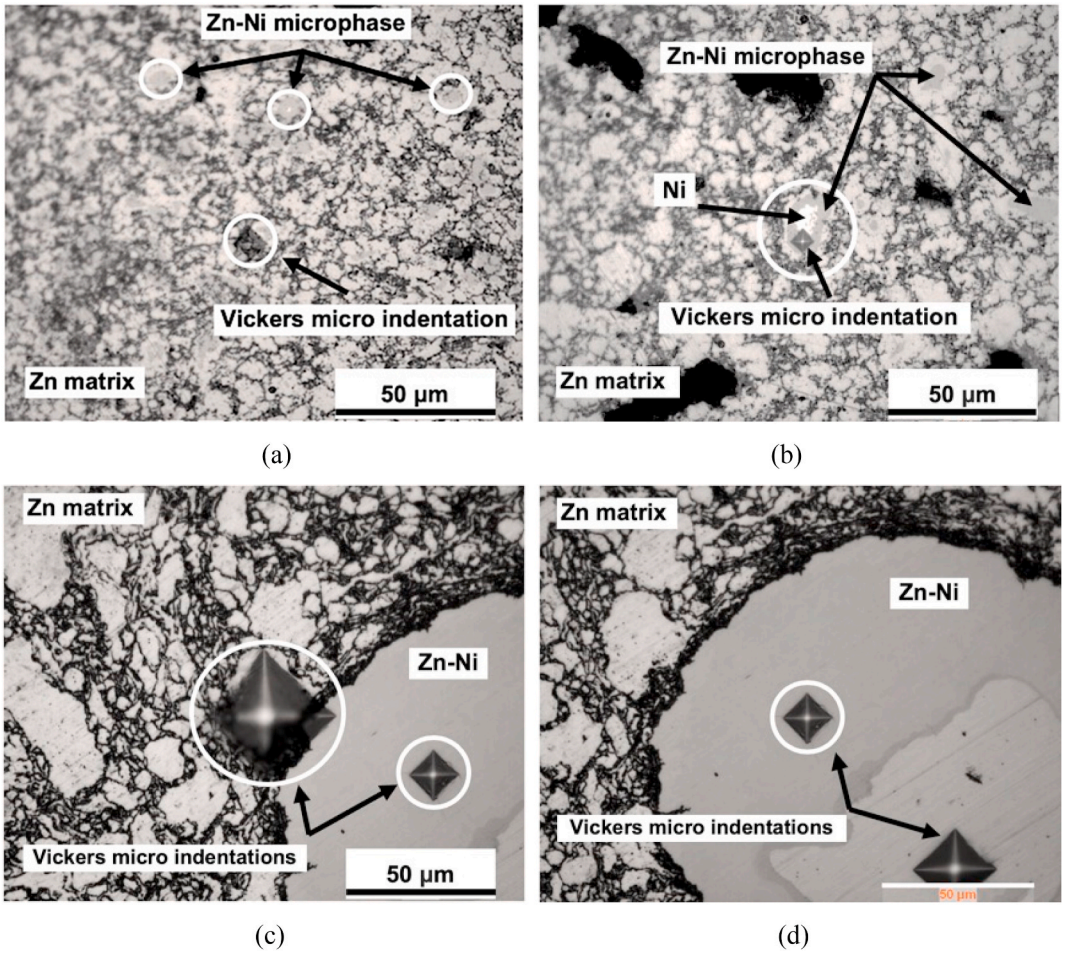

Fig. 11. Vickers indentations of Zn–Ni$_{15}$ alloys (400× magnification) in different phases of the materials synthesized with Ni nanoparticles (a–b) and Ni microparticles (c–d).

positive effect on the elastic behavior because the E_{us} values were reduced in all the combinations compared to the reference value of E_{us} in the pure Zn (82 ± 4 GPa). According to the results, the behavior of E_{us} in the systems will depend on the particle size of Ni incorporated since when Ni nanoparticles were incorporated the E_{us} values decreased while when microparticles of Ni were incorporated, the E_{us} values increased, this is, according to José G. Miranda-Hernández et al. [37], the E_{us} values of the alloys synthesized with Ni microparticles have similar behavior but with higher values than the values of the alloys synthesized with Ni nanoparticles. Probably the cause of that behavior is related to the hardness values, as the hardness values of materials with Ni nanoparticles were higher than those obtained in the alloys synthesized with Ni microparticles.

4. Conclusions

The synthesis of Zn-Nix alloys, such as Zn–Ni_5, Zn–Ni_{10} Zn–Ni_{15} Zn–Ni_{20} are feasible for additions of Ni nanoparticles by powder metallurgy method using low time in the mechanical milling process and the sintering process.

The results of XRD showed that the intermetallic phases were not formed during the mechanical milling process. However, intermetallic alloys appear after the sintering process due to the mechanics of solid-state diffusion (NiZn, Ni_3Zn_{22}, $NiZn_3$, Ni_5Zn_{21}, δ-NiZn, and ɣ-ZnNi). This behavior is favorable for the synthesis of Zn–Ni alloys because the time used is short.

The changes to the morphology microstructural of the Zn-Nix system are due to the increase of Ni in each composition. Also, the Zn-Nix alloys presented an increase in porosity with the Ni addition. Also, the mechanical properties such as hardness and Young's modulus are a function of the %Ni addition in the Zn-based alloys.

Credit author statement

We notified that all author participates in this work with the same input.

Declaration of competing interest

The authors declare that they have no known competing financial interests or personal relationships that could have appeared to influence the work reported in this paper.

Acknowledgments

Members of the research group Ingeniería Industrial Avanzada (UAEM-CA-202) would like to thank the PFCE-2020 program by its support in the infrastructure provided to strengthen CA, as well as the IPN is appreciatively for its technical support in the SEM micrographs obtained by EDS and XRD analysis. Also, the authors are grateful to CONACyT for its distinction and encouragement as national researcher SNI. Finally, the research group recognizes the participation of Ricardo Miranda as an exceptional collaborator of this work and student of Physics and Mathematics in the Gettysburg College, Pennsylvania, USA.

References

[1] F.M. Azizan, H. Purwanto, M.Y. Mustafa, Effect of Sn addition on mechanical properties of zinc-based alloy, Adv. Mater. Res. 576 (2012) 378–381. https://doi.org/10.4028/www.scientific.net/AMR.576.378.

[2] H.Y. Lee, S.G. Kim, Characteristics of Ni deposition in an alkaline bath for Zn–Ni alloy deposition on steel plates, Surf. Coating. Technol. 135 (2000) 69–74, https://doi.org/10.1016/S0257-8972(00)00731-3.

[3] P. Ganesan, S.P. Kumaraguru, B.N. Popov, Development of Zn–Ni-Cd coatings by pulse electrodeposition process, Surf. Coating. Technol. 201 (2006) 3658–3669, https://doi.org/10.1016/j.surfcoat.2006.08.143.

[4] Heidi A. Conrad, John R. Corbett, Teresa D. Golden, Electrochemical deposition of γ-phase zinc-nickel alloys from alkaline solution, J. Electrochem. Soc. 159 (2011) 10–15. https://doi.org/10.1149/2.027201jes.

[5] G. Barceló, E. García, M. Sarret, C. Müller, J. Pregonas, Characterization of zinc-nickel alloys obtained from an industrial chloride bath, J. Appl. Electrochem. 28 (1998) 1113–1120, https://doi.org/10.1023/A:1003461109203.

[6] M.E.P. Souza, E. Ariza, M. Ballester, I.V.P. Yoshida, L.A. Rocha, C.M.A. Freire, Silicone resin to improve corrosion resistance of Zn and ZnFe coated steel, Materia 11 (2006) 16–23, https://doi.org/10.1590/S1517-70762006000100004.

[7] R. Rizwan, M. Mehmood, M. Imran, J. Ahmad, M. Aslam, Javed I. Akhter, Deposition of nanocrystalline zinc-nickel alloys by D.C. Plating in additive free chloride bath, Mater. Trans. 48 (2007) 1558–1565, https://doi.org/10.2320/matertrans.MER2007022.

[8] J.B. Bajat, M.D. Maksimovic, V.B. Miskovic-Stankovic, S. Zec, Electrodeposition and characterization of Zn–Ni alloys as sublayers for epoxy coating deposition, J. Appl. Electrochem. 31 (2001) 355–361, https://doi.org/10.1023/A:1017580019551.

[9] A. Petrauskas, L. Grinceviciene, A. Cesuniene, E. Matulionis, Stripping of Zn–Ni alloys deposited in acetate-chloride electrolyte under potentiodynamic and galvanostatic conditions, Surf. Coating. Technol. 192 (2005) 299–304, https://doi.org/10.1016/j.surfcoat.2004.08.191.

[10] H. Okamoto, Ni-Zn (Nickel-Zinc), J. Phase Equil. 24 (2003) 280–281, https://doi.org/10.1361/105497103770330695.

[11] E. Mostaed, M. Sikora-Jasinska, A. Mostaed, S. Loffredo, A.G. Demir, B. Previtali, D. Mantovani, R. Beanland, M. Vedani, Novel Zn-based alloys for biodegradable stent applications: design, development and in vitro degradation, J. Mechan, Behav. Biomed. Mater. 60 (2016) 581–602, https://doi.org/10.1016/j.jmbbm.2016.03.018.

[12] C. Gang, L. Klaus-Dieter, C. Peng, An in situ study of NiTi powder sintering using neutron diffraction, Met 5 (2015) 530–546, https://doi.org/10.3390/met5020530.

[13] N. Setoudeh, M.H. Paydar, M. Sajjadnejad, Effect of high energy ball milling on the reduction of nickel oxide by zinc Powder, J. Alloys Compd. 623 (2015) 117–120, https://doi.org/10.1016/j.jallcom.2014.10.085.

[14] S. Bid, S.K. Pradhan, Characterization of the crystalline structure of ball-milled nano-Ni–Zn-ferrite by Rietveld method, Mater. Chem. Phys. 84 (2004) 291–301, https://doi.org/10.1016/j.matchemphys.2003.08.012.

[15] J. Park, W. Kim, C. Suh, S. Kim, Catalytic properties of Ni-Zn alloy prepared by mechanical alloying for steam reforming from methanol, Met. Mater. Int. 18 (2012) 237–241, https://doi.org/10.1007/s12540-012-2006-6.

[16] J.M. Kim, J.S. Park, Microstructure and mechanical properties of TiC nanoparticle-reinforced iron-matrix composites, Strength Mater. 46 (2014) 177–182, https://doi.org/10.1007/s11223-014-9533-y.

[17] Kahtan S. Mohammed, Haider T. Naeem, Effect of Milling parameters on the synthesis of Al-Ni Intermetallic compound prepared by mechanical alloying, The Phys. Met. Metallography 116 (2015) 859–868, https://doi.org/10.1134/S0031918X15090070.

[18] M.A. Ahmed, E. Ateia, L.M. Salah, A.A. El-Gamal, Structural and electrical studies on La3+ substituted Ni–Zn ferrites, Mater. Chem. Phys. 92 (2005) 310–321, https://doi.org/10.1016/j.matchemphys.2004.05.049.

[19] G. Penev Vassilev, T. Gomez-Acebo, T. Jean-Claude, Thermodynamic optimization of the Ni-Zn system, J. Phase Equil. 21 (2000) 287–301, https://doi.org/10.1361/105497100770340075.

[20] T. Lee, Donald S. Shih, Y. Lee, C. Soo Lee, Manufacturing ultrafine-grained Ti-6Al-4V bulk rod using multi-pass caliber-rolling, Metals 5 (2015) 777–789, https://doi.org/10.3390/met5020777.

[21] R. Fratesi, G. Roventi, Corrosion resistance of Zn-Ni alloy coatings in industrial production, Surf. Coating. Technol. 82 (1996) 158–164, https://doi.org/10.1016/0257-8972(95)02668-1.

[22] J. Giridhar, W.J. van Ooij, Study of Zn-Ni and Zn-Co alloy coatings electrodeposited on steel strips II: corrosion, dezincification, and sulfidation of the alloy coatings, Surf. Coating. Technol. 53 (1992) 35–47, https://doi.org/10.1016/0257-8972(92)90101-F.

[23] W.A. Badawy, H. Nady, G.M. Abd El-Hafez, Electrodeposited Zn-Ni alloys as promising catalysts for hydrogen Production-Preparation, characterization, and electrocatalytic activity, J. Alloys Compd. 699 (2017) 1146–1156, https://doi.org/10.1016/j.jallcom.2016.12.228.

[24] Y. Boonyongmaneerat, S. Saenapitak, K. Saengkiettiyut, Reverse pulse electrodeposition of Zn–Ni alloys from a chloride bath, J. Alloys Compd. 487 (2009) 479–482, https://doi.org/10.1016/j.jallcom.2009.07.163.

[25] F.J. Fabri Miranda, I.C.P. Margaret, O.R. Mattos, O.E. Barcia, R. Wiart, Corrosion behavior of zinc-nickel alloy electrodeposited coatings, Corrosion Sci. 55 (1999) 732–742, https://doi.org/10.5006/1.3284028.

[26] V. Viswanathan, T. Laha, K. Balani, A. Agarwal, S. Seal, Challenges and advances in nanocomposite processing techniques, Mater. Sci. Eng. R 54 (2006) 121–285, https://doi.org/10.1016/j.mser.2006.11.002.

[27] Roberto A. Rodríguez-Díaz, Alejandro Sedano, Arturo Molina-Ocampo, Jesús Porcayo-Calderón, Jorge Uruchurtu-Chavarín, Manuel González-Pérez, Production of FeAl nanostructured alloy by mechanical alloying and its microstructural characterization, Avances en Ciencias e Ingeniería 4 (2013) 95–104. https://dialnet.unirioja.es/servlet/articulo?codigo=4710379.

[28] K. Hyun-Su, L. Seok-Jae, S. In-Jin, Rapid synthesis and consolidation of nanostructured (Mo, W)Si2 by high-frequency induction heated sintering and its mechanical properties, J. Ceram. Process. Res. 15 (2014) 286–289. http://www.jcpr.or.kr/journal/archive/view/1574.

[29] C. Carreño-Gallardo, I. Estrada-Guel, M. Romero-Romo, R. Cruz-Garcia, C. Lopez-Melendez, R. Martinez-Sanchez, Characterization of Al2O3NP–Al2024 and

AgCNP–Al2024 composites prepared by mechanical processing in a high-energy ball mill, J. Alloys Compd. 536 (2012) S26–S30, https://doi.org/10.1016/j.jallcom.2011.12.010.

[30] Edval G. Araujo, Ricardo M. Leal Neto, Marina F. Pillis, Francisco Ambrózio Filho, High energy ball milling processing, Mater. Sci. Forum 416 (4) (2003) 128–133. https://doi.org/10.4028/www.scientific.net/MSF.416-418.128.

[31] H. Herraiz-Cardona, E. Ortega, V. Peréz-Herranz, Impedance study of hydrogen evolution on Ni/Zn and Ni-Co/Zn stainless steel based electrodeposits, Electrochem. Acta 56 (2011) 1308–1315, https://doi.org/10.1016/j.electacta.2010.10.093.

[32] M.J. De Giz, A.S. Machado, L.A. Avaca, E.R. Gonzalez, High area Ni-Zn and Ni-Co-Zn co-deposits as hydrogen electrodes in alkaline solutions, J. Appl. Electrochem. 22 (1992) 973–977, https://doi.org/10.1007/BF01024146.

[33] J. Divised, H. Schmitz, J. Balej, Ni and Mo coatings as hydrogen cathodes, J. Appl. Electrochem. 19 (1989) 519–530, https://doi.org/10.1007/BF01022108.

[34] J.C. Sabol, W.Z. Misiolek, A. Oztekin, S. Neti, Characterization of intermediate phases formed between solid nickel and liquid zinc during use as an encapsulated phase change material in solar thermal energy storage systems, Metallogr. Microstruct. Anal. 1 (2012) 208–216, https://doi.org/10.1007/s13632-012-0035-7.

[35] W. Xiong, H. Xu, Y. Du, Thermodynamic investigation of the galvanizing systems, II: thermodynamic evaluation of the Ni–Zn system, Calphad 35 (2011) 276–283, https://doi.org/10.1016/j.calphad.2011.03.003.

[36] H. Tawfiq Naeem, The effects of nickel additions on microstructural and hardness of ball-milled of l-6wt%, Zn-3wt%, Mg-2wt%, Cu alloys underwent the artificial aging, J. Asian Sci. Res. 6 (2016) 158–168, https://doi.org/10.18488/journal.2/2016.6.12/2.12.158.168.

[37] José G. Miranda-Hernández, Héctor Herrera-Hernández, Carlos O. González-Morán, Jesús Noé Rivera Olvera, Ivanovich Estrada-Guel, Fabián Botello Villa, Synthesis and characterization of Zn-nix advanced alloys prepared by mechanical milling and sintering at solid-state process, Ann. Mater. Sci. Eng. (2017) 1–12, https://doi.org/10.1155/2017/7967848, 2017.

[38] J.A. Aragón, J.R. Miranda, I. Hilerio D. Muñoz, R. Hernandez, V. Cortés, A. Altamirano, Compuestos de matriz metálica rica en Zn, con alto contenido de Al y componentes estructurales de compuestos intermetálicos de Cu-Zn y Cu-Al particulados, Rev. Mexic. Fisica 53 (2007) 105–113. https://rmf.smf.mx/ojs/rmf/article/view/3519/3486.

[39] J.A. Aragón, J.R. Miranda, Materiales compuestos de matriz metálica rica en Zn con alto contenido de Al y componente estructural de ZnO, Rev. Mexic. Fisica 51 (2005) 356–364. https://rmf.smf.mx/ojs/rmf/article/view/3380/3347.

[40] G. Rodríguez-Castro, Campos-Silva, E. Chávez-Gutiérrez, J. Martínez-Trinidad, E. Hernández-Sánchez, A. Torres-Hernández, Mechanical properties of FeB and Fe_2B layers estimated by Berkovich nanoindentation on tool borided steel, Surf. Coating. Technol. 215 (2013) 291–299, https://doi.org/10.1016/j.surfcoat.2012.05.145.